Gapless spin excitations in superconducting $La_{2-x}Ca_{1+x}Cu_2O_6$ with T_c up to 55 K

John A. Schneeloch,[1,2,*] Ruidan Zhong,[1,3,†] M. B. Stone,[4] I. A. Zaliznyak,[1] G. D. Gu,[1]
Guangyong Xu,[1,‡] and J. M. Tranquada[1]

[1]*Condensed Matter Physics and Materials Science Division, Brookhaven National Laboratory, Upton, New York 11973, USA*
[2]*Department of Physics and Astronomy, Stony Brook University, Stony Brook, New York 11794, USA*
[3]*Materials Science and Engineering Department, Stony Brook University, Stony Brook, New York 11794, USA*
[4]*Neutron Scattering Division, Oak Ridge National Laboratory, Oak Ridge, Tennessee 37831, USA*

We report inelastic neutron scattering on single crystals of the bilayer cuprate family $La_{2-x}Ca_{1+x}Cu_2O_{6+\delta}$, including two crystals made superconducting (transitions at 45 and 55 K) by high-pressure annealing in an oxygen-containing atmosphere. The magnetic excitations in the nonsuperconducting crystal have a similar temperature dependence as those in weakly hole-doped cuprates. In the superconducting crystals, there is a near-uniform suppression of the magnetic spectral weight with increasing temperature; in particular, there are no signs of a spin gap or "resonance" peak. This is different from the temperature dependence seen in many optimally doped cuprates but similar to the behavior seen in certain underdoped cuprates. We discuss the possible connection with pair-density-wave superconductivity.

I. INTRODUCTION

While the mechanism of superconductivity in the high-T_c cuprate superconductors remains controversial, inelastic neutron-scattering measurements of magnetic correlations may give insight into excitations widely believed to play an important role in cuprate superconductivity. The cuprates consist of many families, each having CuO_2 planes and a similar phase diagram [1], but each also having quirks such as differing numbers of CuO_2 planes per unit cell, interlayer structures, type and mobility of dopants, etc. It is important to conduct measurements on many different cuprate families to distinguish between properties universal to all cuprates or particular to certain families. One family infrequently studied by neutrons is the $La_{2-x}(Ca,Sr)_xCaCu_2O_{6+\delta}$ (La-2126) family [2–6], which is a bilayer variant of the more commonly studied "La-214" family having La_2CuO_4 as the parent compound.

Synthesis of large, superconducting La-2126 crystals is difficult, as substitution of Ca or Sr for La at sufficient levels to yield superconductivity requires annealing in a high-pressure oxygen-containing atmosphere [7,8], and such facilities are relatively uncommon. We have recently succeeded in growing and oxygen-annealing large crystals of Ca-doped La-2126, achieving superconducting transition temperatures, T_c, as high as 55 K [9–11]. In contrast to La-214, the La-2126 structure contains CuO_2 bilayers. A transport study on La-2126 crystals demonstrated decoupling of the superconducting bilayers in a magnetic field applied perpendicular to the layers [12]. In this paper, we investigate the spin excitations in similar crystals.

There are a number of commonly observed responses in the cuprates. In the insulating parent compounds, antiferromagnetic spin waves disperse from magnetic Bragg peaks characterized by wave vector $\mathbf{Q}_{AF} = (0.5, 0.5, 0)$ [13]. With increasing hole doping, the dispersion of the magnetic excitations tends to transform into an "hourglass" shape with incommensurate excitations at low energies, as has been observed in $La_{2-x}Ba_xCuO_4$ (LBCO), $La_{2-x}Sr_xCuO_4$, $YBa_2Cu_3O_{6+\delta}$ (YBCO), and $Bi_2Sr_2CaCu_2O_{8+\delta}$ [14]. In optimally doped cuprates, a spin gap is present below T_c, and a putative resonance peak is typically observed above the gap [15–18]. The spin gap appears to be a common feature of cuprates with a spatially uniform superconducting state [19].

With sufficient underdoping, however, there are several cases where the spin gap and resonance are not observed; instead, gapless spin fluctuations coexist with superconductivity. Examples include $YBa_2Cu_3O_{6.45}$ with $T_c = 35$ K [20], $La_{1.93}Sr_{0.07}CuO_4$ with $T_c = 20$ K [21], and $La_{1.905}Ba_{0.095}CuO_4$ with $T_c = 32$ K [22]. In the latter case, decoupling of the superconducting layers has been observed over a considerable range of c-axis magnetic field [23,24]. The field-induced state is similar to the two-dimensional superconductivity detected at zero field in $La_{1.875}Ba_{0.125}CuO_4$ [25], which has been attributed to pair-density-wave (PDW) superconducting order [26,27]. Is a similar story relevant to La-2126?

Previous neutron-scattering measurements on La-2126 have focused on the elastic scattering of unannealed crystals that were non- or weakly superconducting [29,30]. These measurements showed long-range antiferromagnetic (AF) order in $La_{1.9}Ca_{1.1}Cu_2O_{6+\delta}$ and short-range AF order in

TABLE I. Sample labels, superconducting transition temperatures T_c, along with incident neutron energies E_i, and corresponding T_0 and F_1 chopper frequencies used for the low-energy (LE) and high-energy (HE) configurations. Also included are the energy resolution ΔE (full width at half maximum at $\hbar\omega = 0$) and $\Delta E/E_i$ [28].

Sample	T_c (K)	LE					HE				
		E_i (meV)	T_0 (Hz)	F_1 (Hz)	ΔE (meV)	$\Delta E/E_i$	E_i (meV)	T_0 (Hz)	F_1 (Hz)	ΔE (meV)	$\Delta E/E_i$
NSC	0	60	90	180	3.6	0.060	150	90	300	7.9	0.053
SC45	45	40	30	180	2.1	0.052	120	60	240	7.5	0.062
SC55	55	60	90	180	3.6	0.060	150	90	300	7.9	0.053

$La_{1.85}Sr_{0.15}CaCu_2O_{6+\delta}$, with the order appearing to be commensurate in both cases [30]. A tetragonal-to-orthorhombic structural phase transition upon cooling has been observed for both $La_{2-x}Sr_xCaCu_2O_{6+\delta}$ and $La_{2-x}Ca_{1+x}Cu_2O_{6+\delta}$ [29,30].

In this paper, we present an inelastic neutron-scattering study of $La_{2-x}Ca_{1+x}Cu_2O_6$ single crystals, two of which exhibit bulk superconductivity induced by high-pressure oxygen annealing. We have previously characterized the structures of these crystals [10,31]. The annealing appears to enhance the Ca concentration of the La-2126 phase into the superconducting regime, at the cost of creating some effective intergrowths of two other cuprate phases, as we explain below. Nevertheless, only the La-2126 phase has bilayers, the spin excitations of which have a modulated structure factor that allows us to separate them from other contributions. Our key findings are (1) the absence of a spin gap in the superconducting state and (2) a robust superexchange energy, despite considerable softening with doping.

The rest of the paper is organized as follows. The materials and methods are described in the next section, followed by some background on the acoustic and optical magnon modes expected in a bilayer cuprate. The data and analysis are presented in Sec. IV. We discuss the connection with intertwined orders in Sec. V, and end with a summary.

II. MATERIALS AND METHODS

The details of the growth, annealing, and characterization of crystals of $La_{2-x}Ca_{1+x}Cu_2O_6$ with nominal values of $x = 0.1$ and 0.15 are described in [10,12,31]. In the present paper, two crystals of $x = 0.1$ were studied: sample NSC (mass of 7.5 g) was as-grown and nonsuperconducting, while sample SC45 (6.3 g) was annealed in high-pressure oxygen (pressure above 0.55 GPa and $T > 1130\,^{\circ}$C) and had a superconducting transition temperature $T_c = 45$ K (determined by magnetization). Crystal SC55 (7.4 g) corresponds to nominal $x = 0.15$, with similar annealing conditions, and $T_c = 55$ K.

While the NSC sample appears to be single phase, detailed electron-diffraction [31] and neutron-diffraction [10] studies demonstrated that the annealing induces the formation of intergrowthlike domains of La_2CuO_4 and $La_8Cu_8O_{20}$. The volume fraction of the superconducting La-2126 phase was estimated to be ~70% [10]. It was inferred that the segregation of the La_2CuO_4 and $La_8Cu_8O_{20}$ phases caused an enrichment of the Ca concentration in the remaining La-2126 phase, so that the hole concentration in the CuO_2 bilayers is tuned by Ca substitution for La rather than by interstitial oxygen. While it would be desirable to determine the actual

Ca concentration in the La-2126 superconducting phase, doing so is complicated by the unusual heterostructures of these samples.

Inelastic neutron-scattering experiments were performed on the SEQUOIA time-of-flight spectrometer at the Spallation Neutron Source, Oak Ridge National Laboratory [32,33]. For each sample, two incident energies E_i were used, a low-energy choice and a high-energy choice. These are listed in Table I, along with the corresponding settings for the T_0 and Fermi (F_1) chopper frequencies. The different E_i choices for SC45 vs NSC and SC55 were made in separate experimental runs. For simplicity, from here on we will refer to the LE and HE configurations as defined in the table.

To index the scattering, we use a pseudotetragonal unit cell with lattice parameters $a = 3.83$ Å and $c = 19.36$ Å. All wave vectors are reported in reciprocal-lattice units. Each sample was oriented with $\mathbf{Q} = (H, 0, L)$ in the horizontal plane and $(0, K, 0)$ in the vertical direction. For each measurement, the sample was rotated over at least $90°$ in $1°$ steps. The collected data were then mapped into the region of $H \geqslant 0$, $K \geqslant 0$, and $L \geqslant 0$ by reflection across $H = 0$, $K = 0$, and $L = 0$ and averaged (unless otherwise noted). Errorbars represent statistical error and correspond to one standard deviation from the observed value. Data in the false-color intensity maps have been smoothed, and white regions indicate areas outside of the detector coverage.

For this paper, we will present the inelastic-scattering data in the form of the dynamical scattering function $S(\mathbf{Q}, \omega)$ defined by the quantity $\tilde{M}(\mathbf{Q}, \omega)$ in Eq. (10) of [34], with the exceptions that we will not correct for the magnetic form factor (and the Debye-Waller factor is ignored). A common way to determine the absolute magnitude of $S(\mathbf{Q}, \omega)$ is to normalize to measurements of incoherent elastic scattering from a standard vanadium sample. As we only had vanadium data for the measurement conditions used for the SC45 sample, we used the following normalization procedure. First, for the SC45 crystal with the LE configuration and $T = 4$ K, the neutron-scattering intensity of the (200) longitudinal acoustic phonon at $\hbar\omega = 6$ meV was measured and used to calculate the quantity NR_0k_f, where N is the number of Cu ions, R_0 is the resolution volume, and k_f is the outgoing neutron wave-vector magnitude [34]. [Similar values of NR_0k_f (within ~20%) were obtained using vanadium data.] Next, intensities of the NSC and SC55 data in the LE configuration were scaled relative to the SC45 data using acoustic phonon intensities at (107) and $T = 4$ K. As it was not possible to resolve the separate phonon branches near (107), all of the spectral weight within $5.5 \leqslant \hbar\omega < 6.5$ meV, $0 \leqslant K < 0.2$, and

$6.5 \leqslant L < 7.5$ was averaged and integrated along H after subtracting a background obtained from fitting a sloped line to surrounding data. Finally, the HE-configuration data were normalized for each crystal relative to their LE data by comparing averages of incoherent scattering found at $(0.15,0.825,0)$, $(0.25,0.825,0)$, $(0.35,0.825,0)$, $(0.35,0.75,0)$, and $(0.5,0.15,0)$ at $T = 4$ K.

While we have not corrected for the magnetic form factor in evaluating $S(\mathbf{Q}, \omega)$, we will correct for it when converting to the imaginary part of the dynamic spin susceptibility, $\chi''(\mathbf{Q}, \omega)$. As a result, the effective relationship used here is

$$\chi''(\mathbf{Q}, \omega) = \left[\frac{\pi (1 - e^{-\hbar\omega/kT})}{2f^2(\mathbf{Q})} \right] S(\mathbf{Q}, \omega), \qquad (1)$$

where $f(\mathbf{Q})$ is the magnetic form factor calculated for La_2CuO_4 in the same fashion as that for Sr_2CuO_3 analyzed in [35]. This formula essentially corresponds with Eq. (13) of [34].

III. BACKGROUND

For small x, $La_{2-x}(Ca,Sr)_xCaCu_2O_6$ exhibits antiferromagnetic order with ordering wave vector $\mathbf{Q}_{AF} = (0.5, 0.5, 1)$ [29,30]. This involves antiparallel nearest-neighbor Cu spins in all directions within CuO_2 bilayers, similar to the order in $YBa_2Cu_3O_{6+x}$ [36]. The coupling between neighboring layers causes the bilayer spin waves to split into acoustic and optical modes, where the oscillations in neighboring layers are correspondingly in-phase and antiphase [37]. These modes have structure factors proportional to $\sin(\pi z'L)$ and $\cos(\pi z'L)$, respectively, where $z'c$ is the separation between Cu atoms along the c axis, $z' = 0.170$ [38], and the scattered intensity is proportional to the square of the structure factor. For the acoustic mode, the intensity is zero at $L = 0$ and 5.9, but a maximum at $L \approx 2.9$ [30], with the minima and maxima reversing for the optical mode. The optical magnon mode should have a significant energy gap; in antiferromagnetic $YBa_2Cu_3O_{6+x}$, the gap is ~ 70 meV [39,40], and it decreases in energy with doping [41].

Now, the bilayer spin fluctuations from the La-2126 phase are not the only source of scattering that may occur along $\mathbf{Q} = (0.5, 0.5, L)$. For example, the apical oxygens tend to be modulated at the same in-plane wave vector [29], and we also have, in SC45 and SC55, a contribution from the antiferromagnetic correlations in the La-214 phase [10]. Spin fluctuations from the La-214 phase should vary monotonically with L, while the structure factor for the La-2126 apical-oxygen modulation is weak at small Q and distinct from that of the bilayer spin fluctuations. Hence, in order to identify the latter, it is important to measure the $\mathbf{Q}$ dependence of the spin fluctuations in three dimensions, which one can do with the rotating crystal method [42]. At lower energies, we can identify the La-2126 spin fluctuations from the $\sin^2(\pi z'L)$ intensity modulation, and at higher energies we can use the loss of the modulation as a signature of the optical magnon gap.

IV. DATA AND ANALYSIS

Figure 1 shows the dispersion of magnetic excitations along $\mathbf{Q} = (H, 0.5, 3)$ at low energies for all three samples.
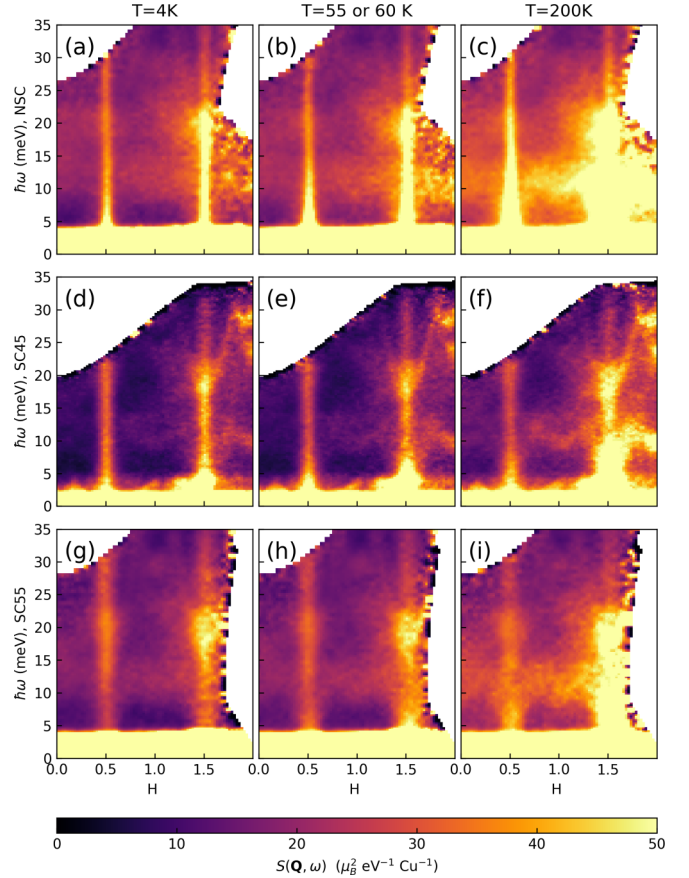

FIG. 1. Color maps of $S(\mathbf{Q}, \omega)$ obtained in the LE configuration as a function of excitation energy and $\mathbf{Q} = (H, 0.5, 3)$ for NSC (a–c), SC45 (d–f), and SC55 (g–i) at temperatures of 4 K (a, d, g) and 200 K (c, f, i) for all samples, 55 K for SC45 (e), and 60 K for NSC (b) and SC55 (h). Data have been averaged within $2 \leqslant L \leqslant 4$ and $0.4 \leqslant K \leqslant 0.6$. One can see the magnetic excitations dispersing steeply from $H = 0.5$ and 1.5.

Taking account of the expected acoustic mode structure factor for the CuO_2 bilayers (discussed in the previous section), the intensity has been averaged over the range $2 \leqslant L \leqslant 4$. The dispersion about $H = 0.5$ and 1.5 is unresolved because of the large effective spin-wave velocity. With increasing H, superimposed phonon scattering grows in intensity. Of particular note is the dispersive optical phonon mode with a minimum energy of 18 meV at $H = 1.5$, with a strong resemblance to the feature reported in lightly doped $La_{2-x}Ba_xCuO_4$ [43].

To view the in-plane spin correlations, Fig. 2 shows intensity slices in the $(H, K, 3)$ plane, where the energy has been averaged over the range of 8 to 16 meV. (Note that we have averaged the data to improve statistics, and that nothing different from the average is apparent in any slices over smaller energy ranges.) For the NSC sample, the signal is relatively round and narrow. For the superconducting samples, the scattering is broader and adopts a diamond shape. While no incommensurate structure is resolved, the orientation of the diamond is consistent with the incommensurability commonly observed in sufficiently underdoped cuprate superconductors [44]. The lower row of Fig. 2 shows fits to the data with four incommensurate peaks, with peak width constrained to
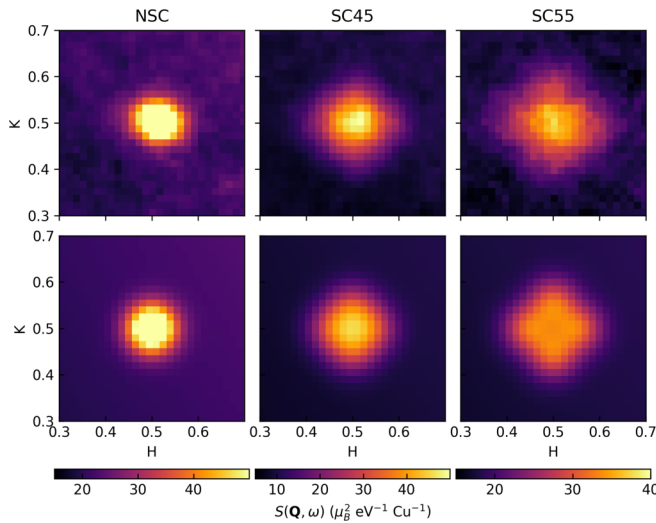
FIG. 2. Top row: Color maps of $S(\mathbf{Q}, \omega)$ in the $(H, K, 3)$ plane centered on the magnetic excitations at $(0.5, 0.5, 3)$. Data have been averaged within $2 \leqslant L \leqslant 4$ and $8 \leqslant \hbar\omega \leqslant 16$ meV. All data were taken at 4 K, with the LE configuration. Bottom row: Fits with four incommensurate Gaussian peaks split about $(0.5, 0.5)$, assuming FWHM $= 0.083$ rlu (obtained from fitting a single Gaussian to the NSC result). The incommensurabilities are 0.007(5), 0.044(1), and 0.056(1) for NSC, SC45, and SC55, respectively.

match that of the NSC data. (Since we cannot actually resolve incommensurate features in the data, a more elaborate analysis does not seem justified.) The pattern found is similar to that observed in underdoped and twinned YBa$_2$Cu$_3$O$_{6+x}$ [45]; in detwinned YBa$_2$Cu$_3$O$_{6+x}$, the incommensurate splitting is almost resolvable at 3 meV [20]. The incommensurabilities fit to our superconducting samples are comparable to those for YBa$_2$Cu$_3$O$_{6+x}$ with $p \sim 0.08$–0.09 [44,46,47].

The magnetic dispersion to higher energies is shown in Figs. 3(a)–3(c). Optical phonons extend up to ~ 85 meV, but the excitations above that are purely magnetic. The higher-energy magnetic excitations are readily apparent in NSC; they are weaker for SC45 and SC55 because of increased Q width and damping from the doped holes, but one can see the roughly vertical dispersion of these excitations at lower energies, where they overlap with phonons. Constant-energy slices at $\hbar\omega = 110$ meV (averaged over a 20-meV window) are presented in Figs. 3(d)–3(f). For NSC, we observe a ring, representing a cut through the conical dispersion of spin waves, the slope of which is proportional to the in-plane superexchange energy J. For SC45 and SC55, the ring has expanded, indicating a decrease in the effective J consistent with previous cuprate results [48,49]. Figure 4 shows radial averages of the rings. The Gaussian fits yield $\mathbf{q}_0 = 0.061(3)$, 0.115(8), and 0.128(6) rlu for NSC, SC45, and SC55, respectively, with half widths of 0.048, 0.062, and 0.071 rlu. From the ratio (110 meV)/Q_0 we can get an estimate of the spin-wave velocity and the effective J. We will discuss this evaluation later, as we must take account of both the acoustic and optic fluctuations. For now, let us denote the effective J by the T_c of the sample; then we note that $J_{45}/J_0 = 0.53(5)$ and $J_{55}/J_0 = 0.48(3)$.
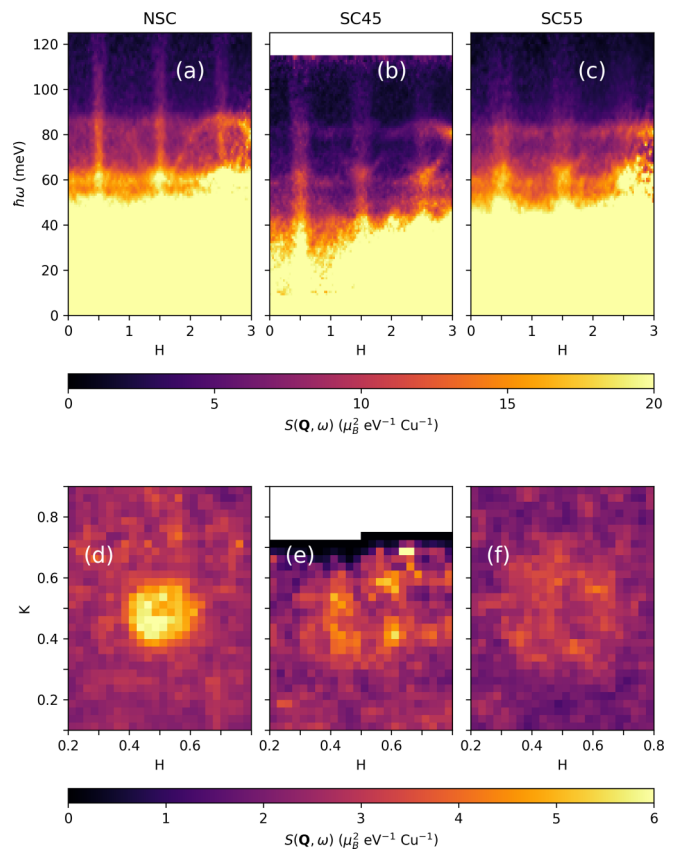

FIG. 3. Color maps of $S(\mathbf{Q}, \omega)$ obtained in the HE configuration at $T = 4$ K along $\mathbf{Q} = (H, 0.5, \langle L \rangle)$ for (a) NSC, (b) SC45, and (c) SC55. Data averaged within $0.4 \leqslant K \leqslant 0.6$ and within the full range of L available for each H and $\hbar\omega$ value. (d–f) Corresponding constant-energy slices in the $(H, K, \langle L \rangle)$ plane at $\hbar\omega = 110$ meV. Data averaged within $100 \leqslant \hbar\omega \leqslant 120$ meV and the full range of available L values (roughly $14 \leqslant L \leqslant 19$ for SC45 and $11 \leqslant L \leqslant 21$ for NSC and SC55).

To verify the acoustic magnon structure factor anticipated at low energies, we plot on the left-hand side of Fig. 5 representative constant-energy slices of intensity in the $(H, 0.5, L)$ plane; cuts along $H = 0.5$ and 1.5 are presented on the right-hand side. The data presented are for SC45 at $T = 4$ K, but the results for the other samples and at temperatures up to 200 K show similar behavior. For $\hbar\omega = 8$, 12, 16, and 24 meV, one
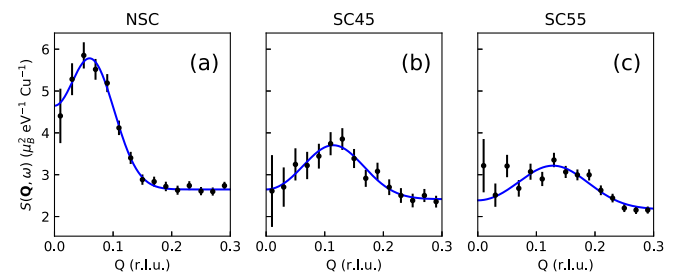

FIG. 4. (a–c) Radial average of $\mathbf{q} = (H, K, \langle L \rangle) - (0.5, 0.5, \langle L \rangle)$ for the 110-meV data in Figs. 3(d)–3(f), respectively. Circles with error bars, data; blue line, Gaussian fit. For the fits, a pair of identical peaks at $\pm Q_0$ were used.
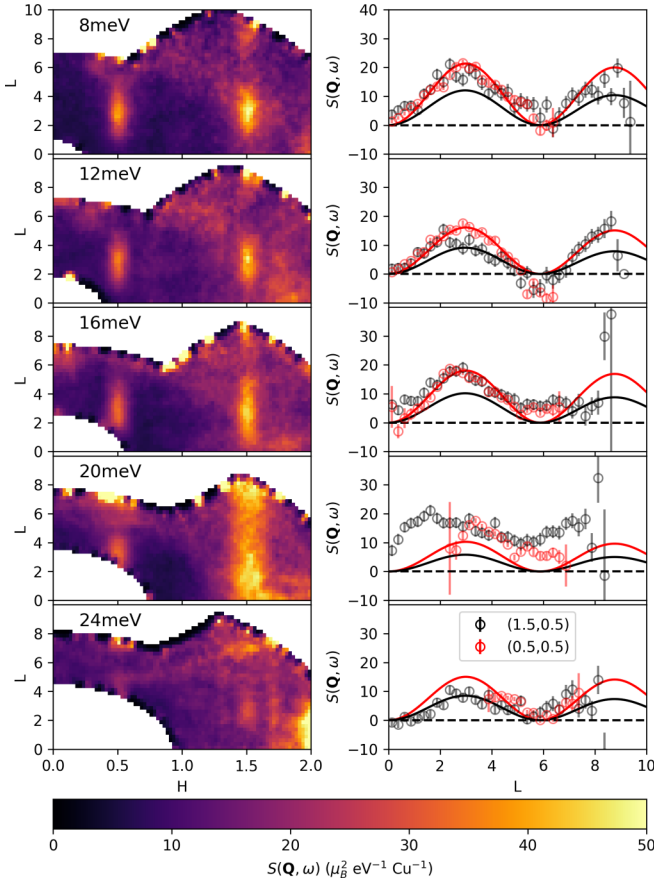
FIG. 5. $S(\mathbf{Q}, \omega)$ for SC45, showing the magnetic scattering along $(0.5, 0.5, L)$ and $(1.5, 0.5, L)$. Left column: Constant-energy maps in the $(H, 0.5, L)$ plane, averaged within $0.4 \leqslant K \leqslant 0.6$ and within $\Delta(\hbar\omega) = \pm 1$ meV around the energy transfers noted at the upper left of each panel (8 to 24 meV in 4-meV steps). Data were taken at $T = 4$ K and $E_i = 40$ meV. Right column: Corresponding intensities of the magnetic excitations along L, averaged within $0.4 \leqslant K \leqslant 0.6$, $0.4 \leqslant H \leqslant 0.6$ for red circles and $1.4 \leqslant H \leqslant 1.6$ for black circles, after subtraction of background determined at neighboring wave vectors. Solid lines correspond to $f^2(\mathbf{Q}) \sin^2(\pi z'L)$ using the Cu form factor determined in [35].

can see that the scattered intensity is sinusoidally modulated, with a maximum at $L \approx 3$ and minima at $L = 0$ and 6, as expected. The only exception is at $\hbar\omega = 20$ meV, where overlapping scattering from an optical phonon dominates the response. We also note that, for $\hbar\omega = 8$ and 16 meV, the intensities at $H = 1.5$ are closer to those at $H = 0.5$ than expected for the form factor dependence.

When the optical magnon branch appears at higher energies, it should have an intensity maximum at $L = 6$, where the acoustic structure factor is zero. To look for the onset of the optical mode, we plot the intensity at $\mathbf{Q}_{op} = (0.5, 0.5, 6)$ and at a background point $\mathbf{Q}_b$ as a function of $\hbar\omega$ for each sample in Figs. 6(a)–6(c). Consistent with expectations, we see that the signal at $\mathbf{Q}_{op}$ matches that at $\mathbf{Q}_b$ for low energies but rises above background at higher energies. To see this more clearly, we plot the difference in intensities at $\mathbf{Q}_{op}$ and $\mathbf{Q}_b$ in Figs. 6(d)–6(f). From these results, we estimate an optical magnon gap Δ_{op} of 53 ± 5, 38 ± 5, and 33 ± 5 meV for NSC, SC45, and SC55, respectively.

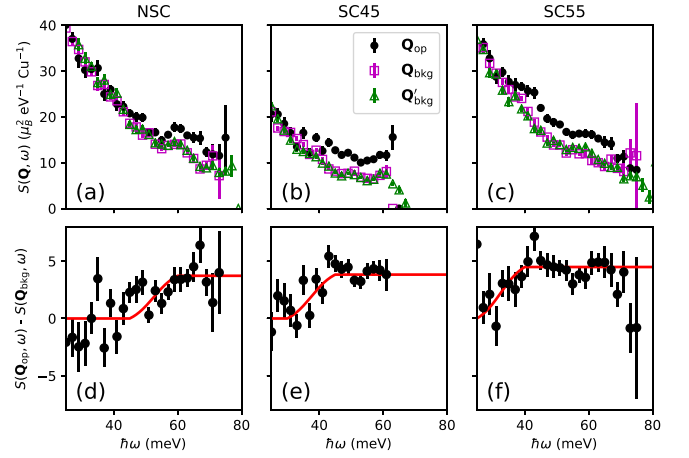
FIG. 6. (a, b, c) $S(\mathbf{Q}, \omega)$ vs $\hbar\omega$ at $\mathbf{Q}_{op} = (0.5, 0.5, 6)$ (filled black circles), along with background intensity at $\mathbf{Q}_{bkg} = (0.3, 0.5, 6)$ (open magenta squares) and $\mathbf{Q}'_{bkg} = (0.7, 0.5, 6)$ (open green triangles). Data were averaged within $0.4 \leqslant H \leqslant 0.6$, $5 \leqslant L \leqslant 7$, and either $0.4 \leqslant K \leqslant 0.6$ for $\mathbf{Q}_{op}$ or $0.2 \leqslant K \leqslant 0.8$ for the background points. (d, e, f) $S(\mathbf{Q}_{op}, \omega)$ after subtraction of averaged background. Red lines are guides to the eye to highlight the increase in intensity with $\hbar\omega$, which is expected due to the presence of the optical branch. Measurements were done with the HE configuration at $T = 4$ K.

For the case of undoped La-2126, where a spin-wave model similar to that for YBa$_2$Cu$_3$O$_6$ [50] should be appropriate, the optical magnon gap, Δ_{op}, should be proportional to $\sqrt{J_\perp J}$, where $J_\perp$ is the effective nearest-neighbor interlayer exchange within bilayers. Taking the square of the ratio of the optical gaps, we find

$$\frac{\Delta_{op}^2(\text{SC45})}{\Delta_{op}^2(\text{NSC})} = 0.51(13) = \frac{J_{45\perp}J_{45}}{J_{0\perp}J_0} \approx \frac{J_{45}}{J_0} \quad (2)$$

and

$$\frac{\Delta_{op}^2(\text{SC55})}{\Delta_{op}^2(\text{NSC})} = 0.39(12) = \frac{J_{55\perp}J_{55}}{J_{0\perp}J_0} \approx \frac{J_{55}}{J_0}. \quad (3)$$

From this analysis, it appears that the doping dependence of Δ_{op} is fully accounted for by the change in J, suggesting that $J_\perp$ is not significantly affected by doping.

Now that we have estimates for Δ_{op}, we can evaluate J from the fits in Fig. 4. We assume that the acoustic branch disperses linearly in q with velocity v. The dispersion of the optical mode is assumed to be $\sqrt{\Delta_{op}^2 + \hbar^2 v^2 q^2}$. For the measurements at 110 meV, both modes should be contributing approximately equally. If $\bar{q}$ is the average peak position, then the velocity should be given by

$$v = \frac{\omega}{2\bar{q}}[1 + \sqrt{1 - (\Delta_{op}/\hbar\omega)^2}]. \quad (4)$$

The theoretical spin-wave velocity for the nearest-neighbor Heisenberg antiferromagnet appropriate to a CuO$_2$ plane is [51]

$$v = \sqrt{2}Z_c Ja/\hbar, \quad (5)$$

where $Z_c = 1.18$. From these formulas and the data for NSC, we obtain $J = 161^{+105}_{-46}$ meV, where we have used half of the
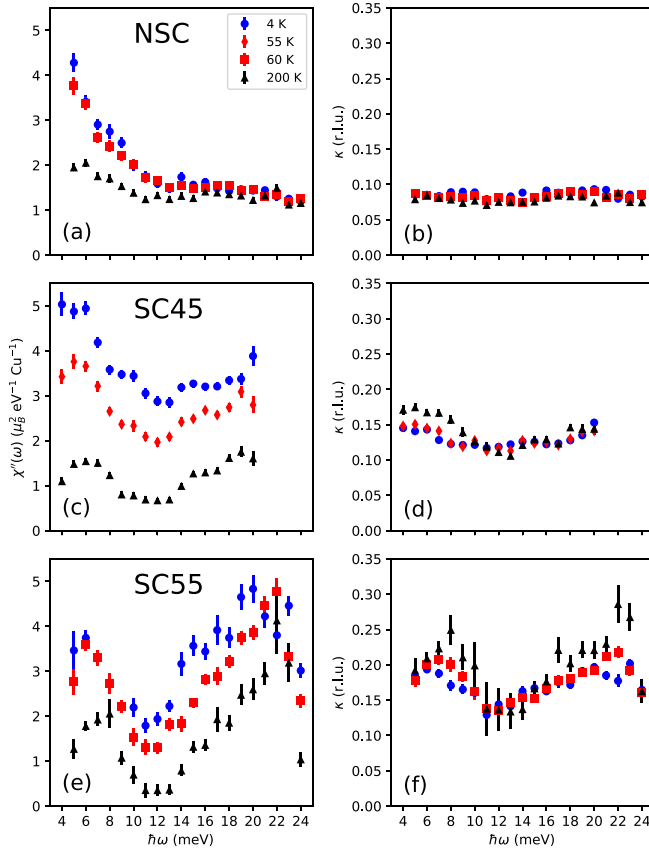
FIG. 7. Fitting results for $\chi''(\omega)$ (a, c, e) and κ (full Q width at half maximum) (b, d, f) for NSC (a, b), SC45 (c, d), and SC55 (e, f), as described in the text. These results are from LE data; measurement temperatures are indicated in the legend.

FIG. 8. Differences of $\chi''(\omega)$ across T_c, with $T = 55$-K (60-K) data subtracted from 4-K data for SC45 (SC55) crystals.

order. The spectrum looks similar to that observed recently in La$_{1.93}$Sr$_{0.07}$CuO$_4$ [21].

For samples SC45 and SC55, the magnetic response is reduced at high temperature and grows on cooling, in a fashion qualitatively similar to that observed in other underdoped cuprate superconductors [20,22,45,53,54]. At low temperature, there is a rise in response at low frequency, which is different from the behavior in cuprates that exhibit a spin gap [18,55–58]. To confirm the change across T_c, we plot the difference between 4 K and $T \gtrsim T_c$ in Fig. 8. As one can see, there is no sign of a spin gap or resonance. The coexistence of superconductivity with gapless spin fluctuations has been observed previously in underdoped La$_{2-x}$Ba$_x$CuO$_4$ [22], La$_{2-x}$Sr$_x$CuO$_4$ [21], and very underdoped YBa$_2$Cu$_3$O$_{6+x}$ [20,53,59].

The width parameter κ, plotted in Figs. 7(b), 7(d) and 7(f), grows with doping but does not show any significant dependence on temperature or energy over this modest energy range. While we have already noted that we cannot resolve any incommensurability, the variation in κ with increasing T_c is consistent with the variation in incommensurability with doping seen in other cuprate superconductors [44].

V. DISCUSSION

The features of the magnetic excitation spectra that we have observed in La-2126 crystals are similar to those observed in various other cuprate systems [14]. For example, the NSC sample exhibits a large spin velocity, indicating an effective J that may be larger than the $J \approx 143$ meV of La$_2$CuO$_4$ [60]; measurements to significantly higher excitation energies would be necessary to reduce the uncertainty in J. The decrease in the magnitude of J with doping is consistent with two-magnon Raman scattering results for other cuprates [48]; the drop by 50% relative to the insulating parent corresponds with optimal doping in La$_{2-x}$Sr$_x$CuO$_4$ and Bi$_2$Sr$_2$CaCu$_2$O$_{8+\delta}$. The decrease in spectral weight at 110 meV with doping follows the trend established by Stock *et al.* [61]: the magnetic spectral weight remains strong at low energies but is depressed on the scale of the pseudogap energy (corresponding to twice the antinodal pseudogap energy identified by photoemission) [62].

The low-energy spin excitations exhibit the bilayer acoustic-mode structure factor previously observed in YBa$_2$Cu$_3$O$_{6+x}$ [50,63] and Bi$_2$Sr$_2$CaCu$_2$O$_{8+\delta}$ [64]. Our result of $\Delta_{op} = 53(5)$ meV can be compared with results for YBa$_2$Cu$_3$O$_{6+x}$ with $x = 0.15$ where $\Delta_{op} = 74(5)$ meV and

half width at half maximum as an estimate of uncertainty in $\bar{q}$. This value of J (with its substantial uncertainty) is on the high side of the distribution of results for other cuprates, but that distribution has a significant width [13].

To characterize the strength of the magnetic excitations as a function of temperature and energy transfer, we took the LE data, integrated it over $2 \leqslant L \leqslant 4$, divided the energy scale into 0.5-meV bins, and fit the scattered signal to the form

$$S(\mathbf{Q}, \omega)/f^2(\mathbf{Q}) = p_0 + \mathbf{p}_1 \cdot \mathbf{Q} + \frac{A}{2\pi\sigma^2} e^{-\frac{1}{2}(\mathbf{Q}-\mathbf{Q_{AF}})^2/\sigma^2}, \quad (6)$$

where the parameters p_0, $\mathbf{p}_1$, $A(\omega)$, and $\sigma(\omega)$ were fit for each $\hbar\omega$ bin, and the full width at half maximum $\kappa = 2\sqrt{2\ln 2}\sigma$. To convert the amplitude to the $\mathbf{Q}$-integrated imaginary part of the dynamic susceptibility, $\chi''(\omega)$, we used

$$\chi''(\omega) = \frac{\pi}{2} A(\omega)(1 - e^{-\hbar\omega/k_B T}). \quad (7)$$

We plot the results for $\chi''(\omega)$ and $\kappa(\omega)$ for each sample at several temperatures in Fig. 7.

For sample NSC, $\chi''(\omega)$ is constant in energy and temperature for $\hbar\omega \gtrsim 10$ meV, consistent with the response observed from spin waves [39,52]. At low $\hbar\omega$, the rise in the signal appears to be a quasielastic response, suggesting local hopping by the low density of doped holes frustrates static
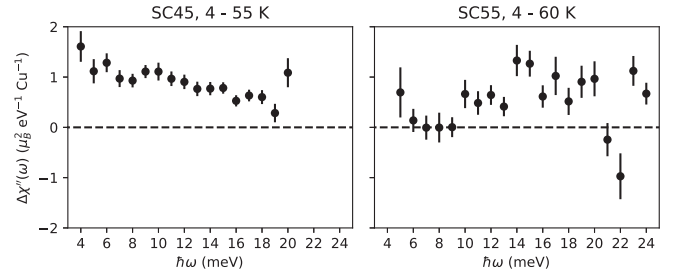
$J = 125(5)$ meV were found [39] (with slightly reduced values reported for a sample with $x = 0.20$ [40]). Our smaller Δ_{op} and larger J in the NSC sample indicate a reduced $J_\perp$ compared to YBCO. On doping $YBa_2Cu_3O_{6+x}$ to $x = 0.5$ ($T_c = 52$ K), Δ_{op} dropped to ~ 59 meV [55], which goes in the same direction as our observations.

For energies below Δ_{op}, the acoustic-mode structure factor allows us to separate the magnetic excitations of La-2126 from a possible contribution from the La-214 intergrowth layers in the annealed crystals, as the latter response should be independent of L. It follows that we have good confidence that our observations of gapless spin fluctuations in SC45 and SC55 correspond to intrinsic features. We certainly see some evolution of the low-energy excitations with doping shown in Fig. 7, as $\chi''(\omega)$ for $\hbar\omega \lesssim 20$ meV is reduced in the superconducting samples at 200 K, with a pronounced dip at 12 meV. Nevertheless, that weight grows on cooling to near T_c, and the difference across T_c (Fig. 8) shows no dip.

There is also an enhancement of $\chi''(\omega)$ at ~ 20 meV in the SC55 sample compared to the NSC sample. This feature appears to be similar to the one identified previously in lightly doped $La_{2-x}Ba_xCuO_4$ by Wagman *et al.* [43], observed in other La-214 samples [19,22], and attributed to spin-phonon hybridization [65]. The apparent absence of such a feature in the NSC sample suggests that the coupling between spin excitations and phonons requires a sufficient level of hole doping. We note that a related gapped-magnon feature with $\hbar\omega \sim 25$ meV was observed in stripe-ordered $La_{1.67}Sr_{0.33}NiO_4$ [66] and confirmed to be magnetic with the use of polarized neutrons [67].

The absence of a spin gap plus the magnetic-field-induced decoupling of superconducting layers [12] parallels such behavior in $La_{2-x}Ba_xCuO_4$ with $x = 0.095$ [22–24]. Of course, there are some differences, as well. In the case of LBCO, there is direct evidence for both spin and charge stripe order [23,68]. For the present samples, we cannot resolve incommensurate peaks in the spin fluctuations, although the data are compatible with broad incommensurate peaks. This situation is similar to YBCO with $x = 0.45$, where detwinned crystals show a clear nematic anisotropy in the magnetic peak widths at low temperature [20]; in that system, incommensurability of the lowest-energy excitations becomes resolvable at higher doping [69,70]. Another issue is the absence of evidence for charge order in La-2126 and YBCO with $x = 0.45$. The lack of evidence does not rule out charge order, but indicates one direction for further study.

As noted in the Introduction, the decoupling of superconducting layers in LBCO, both in zero field for $x = 0.125$

[25] and in applied field for $x = 0.095$ [23,24], has been attributed to PDW order associated with the stripe order [26,27]. So far, direct evidence for PDW order has been limited. The best evidence so far comes from a scanning tunneling spectroscopy study [71] of modulations in vortex halos in $Bi_2Sr_2CaCu_2O_{8+\delta}$, where a specific charge modulation was detected that was predicted to occur when uniform and PDW superconducting orders coexist [72]. For LBCO with $x = 1/8$, phase-sensitive measurements in a Josephson junction provide evidence for a charge-$4e$ response [73], which is another predicted behavior associated with PDW order [74]. A recent high-magnetic-field transport study on the same compound has provided evidence that the charge stripes contain pair correlations even in the absence of phase coherence between neighboring stripes [75].

The nature of superconducting order in La-2126 deserves further attention. While evidence for PDW order is quite indirect, the gapless spin fluctuation spectrum and its temperature dependence seem to indicate that some combination of intertwined orders [76] is involved.

VI. SUMMARY

Three different single crystals of $La_{2-x}Ca_{1+x}Cu_2O_{6+\delta}$ for $x = 0.10$ and 0.15, two of which were made superconducting by high-pressure oxygen annealing, have been studied by inelastic neutron scattering. For the NSC sample, the temperature dependence of the **Q**-integrated $\chi''(\omega)$ was found to be very similar to that of weakly hole-doped cuprates. The superconducting crystals, on the other hand, showed a reduction in $\chi''(\omega)$ with increasing temperature; however, the change in spectral weight across T_c did not show any sign of the spin gap or resonance features seen in many other cuprate superconductors. The lack of these features is consistent with data from underdoped La-214 cuprates. The coexistence of gapless spin fluctuations with superconductivity suggests that intertwined orders are involved. Further work is necessary to test for possible PDW order.

ACKNOWLEDGMENTS

[1] B. Keimer, S. A. Kivelson, M. R. Norman, S. Uchida, and J. Zaanen, From quantum matter to high-temperature superconductivity in copper oxides, Nature (London) **518**, 179 (2015).

[2] R. J. Cava, A. W. Hewat, E. A. Hewat, B. Batlogg, M. Marezio, K. M. Rabe, J. J. Krajewski, W. F. Peck, Jr., and L. W. Rupp, Jr., Structural anomalies, oxygen ordering and superconductivity in oxygen deficient $Ba_2YCu_3O_x$, Physica C **165**, 419 (1990).

[3] A. Fuertes, X. Obradors, J. M. Navarro, P. Gomez-Romero, N. Casañ-Pastor, F. Pérez, J. Fontcuberta, C. Miravitlles, J. Rodriguez-Carvajal, and B. Martínez, Oxygen excess and superconductivity at 45 K in $La_2CaCu_2O_{6+y}$, Physica C **170**, 153 (1990).

[4] K. Kinoshita, H. Shibata, and T. Yamada, High-pressure synthesis of superconducting $La_{2-x}Ca_{1+x}Cu_2O_{6-x/2+\delta}$, Physica C **171**, 523 (1990).

[5] H. B. Liu, D. E. Morris, A. P. B. Sinha, and X. X. Tang, Superconductivity in $La_{2-x}Sr_xCaCu_2O_6$ at 60 K, Physica C **174**, 28 (1991).

[6] K. Kinoshita and T. Yamada, Superconductivity and antiferromagnetism in $La_{2-x}Ca_{1+x}Cu_2O_{6\pm\delta}$ and $La_{2-x}Sr_xCaCu_2O_{6\pm\delta}$, Phys. Rev. B **46**, 9116 (1992).

[7] T. Ishii, T. Watanabe, K. Kinoshita, and A. Matsuda, Single crystal growth and superconductivity in $La_{1.87}Ca_{1.13}Cu_2O_6$, Physica C **179**, 39 (1991).

[8] M. Okuya, T. Kimura, R. Kobayashi, J. Shimoyama, K. Kitazawa, K. Yamafuji, K. Kishio, K. Kinoshita, and T. Yamada, Single-crystal growth and anisotropic electrical properties of $(La_{1-x}Ca_x)_2CaCu_2O_6$, J. Supercond. **7**, 313 (1994).

[9] Xiaoya Shi, I. K. Dimitrov, Toshinori Ozaki, Genda Gu, and Qiang Li, Quasi-two-dimensional fluctuations in the magnetization of $La_{1.9}Ca_{1.1}Cu_2O_{6+\delta}$ superconductors, Phys. Rev. B **96**, 184519 (2017).

[10] J. A. Schneeloch, Z. Guguchia, M. B. Stone, Wei Tian, Ruidan Zhong, K. M. Mohanty, Guangyong Xu, G. D. Gu, and J. M. Tranquada, Growth and structural characterization of large superconducting crystals of $La_{2-x}Ca_{1+x}Cu_2O_6$, Phys. Rev. Materials **1**, 074801 (2017).

[11] G. D. Gu, M. Hücker, Y.-J. Kim, J. M. Tranquada, H. Dabkowska, G. M. Luke, T. Timusk, B. D. Gaulin, Q. Li, and A. R. Moodenbaugh, Crystal growth and superconductivity of $(La_{1-x}Ca_x)_2CaCu_2O_{6+\delta}$, J. Phys. Chem. Solids **67**, 431 (2006).

[12] Ruidan Zhong, J. A. Schneeloch, Hang Chi, Qiang Li, Genda Gu, and J. M. Tranquada, Evidence for magnetic-field-induced decoupling of superconducting bilayers in $La_{2-x}Ca_{1+x}Cu_2O_6$, Phys. Rev. B **97**, 134520 (2018).

[13] J. M. Tranquada, Neutron scattering studies of antiferromagnetic correlations in cuprates, in *Handbook of High-Temperature Superconductivity*, edited by J. R. Schrieffer and J. S. Brooks (Springer, New York, 2007), p. 257.

[14] M. Fujita, H. Hiraka, M. Matsuda, M. Matsuura, J. M. Tranquada, S. Wakimoto, Guangyong Xu, and Kazuyoshi Yamada, Progress in neutron scattering studies of spin excitations in high-T_c cuprates, J. Phys. Soc. Jpn. **81**, 011007 (2012).

[15] Hyungje Woo, Pengcheng Dai, S. M. Hayden, H. A. Mook, T. Dahm, D. J. Scalapino, T. G. Perring, and F. Doğan, Magnetic energy change available to superconducting condensation in optimally doped $YBa_2Cu_3O_{6.95}$, Nat. Phys. **2**, 600 (2006).

[16] H. F. Fong, P. Bourges, Y. Sidis, L. P. Regnault, A. Ivanov, G. D. Gu, N. Koshizuka, and B. Keimer, Neutron scattering from magnetic excitations in $Bi_2Sr_2CaCu_2O_{8+\delta}$, Nature (London) **398**, 588 (1999).

[17] B. Lake, G. Aeppli, T. E. Mason, A. Schröder, D. F. McMorrow, K. Lefmann, M. Isshiki, M. Nohara, H. Takagi, and S. M. Hayden, Spin gap and magnetic coherence in a clean high-temperature superconductor, Nature (London) **400**, 43 (1999).

[18] M. K. Chan, Y. Tang, C. J. Dorow, J. Jeong, L. Mangin-Thro, M. J. Veit, Y. Ge, D. L. Abernathy, Y. Sidis, P. Bourges, and M. Greven, Hourglass Dispersion and Resonance of Magnetic Excitations in the Superconducting State of the Single-Layer Cuprate $HgBa_2CuO_{4+\delta}$ Near Optimal Doping, Phys. Rev. Lett. **117**, 277002 (2016).

[19] Yangmu Li, Ruidan Zhong, M. B. Stone, A. I. Kolesnikov, G. D. Gu, I. A. Zaliznyak, and J. M. Tranquada, Low-energy antiferromagnetic spin fluctuations limit the coherent superconducting gap in cuprates, Phys. Rev. B **98**, 224508 (2018).

[20] V. Hinkov, D. Haug, B. Fauqué, P. Bourges, Y. Sidis, A. Ivanov, C. Bernhard, C. T. Lin, and B. Keimer, Electronic liquid crystal state in superconducting $YBa_2Cu_3O_{6.45}$, Science **319**, 597 (2008).

[21] H. Jacobsen, I. A. Zaliznyak, A. T. Savici, B. L. Winn, S. Chang, M. Hücker, G. D. Gu, and J. M. Tranquada, Neutron scattering study of spin ordering and stripe pinning in superconducting $La_{1.93}Sr_{0.07}CuO_4$, Phys. Rev. B **92**, 174525 (2015).

[22] Zhijun Xu, C. Stock, Songxue Chi, A. I. Kolesnikov, Guangyong Xu, Genda Gu, and J. M. Tranquada, Neutron-Scattering Evidence for a Periodically Modulated Superconducting Phase in the Underdoped Cuprate $La_{1.905}Ba_{0.095}CuO_4$, Phys. Rev. Lett. **113**, 177002 (2014).

[23] Jinsheng Wen, Qing Jie, Qiang Li, M. Hücker, M. v. Zimmermann, Su Jung Han, Zhijun Xu, D. K. Singh, R. M. Konik, Liyuan Zhang, Genda Gu, and J. M. Tranquada, Uniaxial linear resistivity of superconducting $La_{1.905}Ba_{0.095}CuO_4$ induced by an external magnetic field, Phys. Rev. B **85**, 134513 (2012).

[24] Z. Stegen, Su Jung Han, Jie Wu, A. K. Pramanik, M. Hücker, Genda Gu, Qiang Li, J. H. Park, G. S. Boebinger, and J. M. Tranquada, Evolution of superconducting correlations within magnetic-field-decoupled $La_{2-x}Ba_xCuO_4$ ($x = 0.095$), Phys. Rev. B **87**, 064509 (2013).

[25] Q. Li, M. Hücker, G. D. Gu, A. M. Tsvelik, and J. M. Tranquada, Two-Dimensional Superconducting Fluctuations in Stripe-Ordered $La_{1.875}Ba_{0.125}CuO_4$, Phys. Rev. Lett. **99**, 067001 (2007).

[26] A. Himeda, T. Kato, and M. Ogata, Stripe States with Spatially Oscillating d-Wave Superconductivity in the Two-Dimensional $t - t' - J$ Model, Phys. Rev. Lett. **88**, 117001 (2002).

[27] E. Berg, E. Fradkin, E.-A. Kim, S. A. Kivelson, V. Oganesyan, J. M. Tranquada, and S. C. Zhang, Dynamical layer decoupling in a stripe-ordered high-T_c superconductor, Phys. Rev. Lett. **99**, 127003 (2007).

[28] D. L. Abernathy, M. B. Stone, M. J. Loguillo, M. S. Lucas, O. Delaire, X. Tang, J. Y. Y. Lin, and B. Fultz, Design and operation of the wide angular-range chopper spectrometer ARCS at the Spallation Neutron Source, Rev. Sci. Instrum. **83**, 015114 (2012).

[29] C. Ulrich, S. Kondo, M. Reehuis, H. He, C. Bernhard, C. Niedermayer, F. Bourée, P. Bourges, M. Ohl, H. M. Rønnow, H. Takagi, and B. Keimer, Structural and magnetic instabilities of $La_{2-x}Sr_xCaCu_2O_6$, Phys. Rev. B **65**, 220507(R) (2002).

[30] M. Hücker, Young-June Kim, G. D. Gu, J. M. Tranquada, B. D. Gaulin, and J. W. Lynn, Neutron scattering study on $La_{1.9}Ca_{1.1}Cu_2O_{6+\delta}$ and $La_{1.85}Sr_{0.15}CaCu_2O_{6+\delta}$, Phys. Rev. B **71**, 094510 (2005).

[31] Hefei Hu, Yimei Zhu, Xiaoya Shi, Qiang Li, Ruidan Zhong, J. A. Schneeloch, Genda Gu, J. M. Tranquada, and S. J. L. Billinge, Nanoscale coherent intergrowthlike defects in a crystal of $La_{1.9}Ca_{1.1}Cu_2O_{6+\delta}$ made superconducting by high-pressure oxygen annealing, Phys. Rev. B **90**, 134518 (2014).

[32] G. E. Granroth, A. I. Kolesnikov, T. E. Sherline, J. P. Clancy, K. A. Ross, J. P. C. Ruff, B. D. Gaulin, and S. E. Nagler, SEQUOIA: A newly operating chopper spectrometer at the SNS, J. Phys. Conf. Ser. **251**, 012058 (2010).

[33] M. B. Stone, J. L. Niedziela, D. L. Abernathy, L. DeBeer-Schmitt, G. Ehlers, O. Garlea, G. E. Granroth, M. Graves-Brook, A. I. Kolesnikov, A. Podlesnyak, and B. Winn,

A comparison of four direct geometry time-of-flight spectrometers at the Spallation Neutron Source, Rev. Sci. Instrum. **85**, 045113 (2014).

[34] Guangyong Xu, Zhijun Xu, and J. M. Tranquada, Absolute cross-section normalization of magnetic neutron scattering data, Rev. Sci. Instrum. **84**, 083906 (2013).

[35] A. C. Walters, T. G. Perring, Jean-Sebastien Caux, A. T. Savici, G. D. Gu, Chi-Cheng Lee, Wei Ku, and I. A. Zaliznyak, Effect of covalent bonding on magnetism and the missing neutron intensity in copper oxide compounds, Nat. Phys. **5**, 867 (2009).

[36] J. M. Tranquada, D. E. Cox, W. Kunnmann, H. Moudden, G. Shirane, M. Suenaga, P. Zolliker, D. Vaknin, S. K. Sinha, M. S. Alvarez, A. J. Jacobson, and D. C. Johnston, Neutron-Diffraction Determination of Antiferromagnetic Structure of Cu Ions in $YBa_2Cu_3O_{6+x}$ with $x = 0.0$ and 0.15, Phys. Rev. Lett. **60**, 156 (1988).

[37] M. Sato, S. Shamoto, J. M. Tranquada, G. Shirane, and B. Keimer, Two-dimensional Antiferromagnetic Excitations from a Large Single Crystal of $YBa_2Cu_3O_{6.2}$, Phys. Rev. Lett. **61**, 1317 (1988).

[38] K. Kinoshita, F. Izumi, T. Yamada, and H. Asano, Structure refinements of superconducting and nonsuperconducting $La_{1.82}Ca_{1.18}Cu_2O_{6\pm\delta}$ from neutron-diffraction data, Phys. Rev. B **45**, 5558 (1992).

[39] S. M. Hayden, G. Aeppli, T. G. Perring, H. A. Mook, and F. Doğan, High-frequency spin waves in $YBa_2Cu_3O_{6.15}$, Phys. Rev. B **54**, R6905 (1996).

[40] D. Reznik, P. Bourges, H. F. Fong, L. P. Regnault, J. Bossy, C. Vettier, D. L. Milius, I. A. Aksay, and B. Keimer, Direct observation of optical magnons in $YBa_2Cu_3O_{6.2}$, Phys. Rev. B **53**, R14741 (1996).

[41] S. Pailhès, C. Ulrich, B. Fauqué, V. Hinkov, Y. Sidis, A. Ivanov, C. T. Lin, B. Keimer, and P. Bourges, Doping Dependence of Bilayer Resonant Spin Excitations in $(Y, Ca)Ba_2Cu_3O_{6+x}$, Phys. Rev. Lett. **96**, 257001 (2006).

[42] R. A. Ewings, A. Buts, M. D. Le, J. van Duijn, I. Bustinduy, and T. G. Perring, Horace: Software for the analysis of data from single crystal spectroscopy experiments at time-of-flight neutron instruments, Nucl. Instr. Meth. Phys. Res. A **834**, 132 (2016).

[43] J. J. Wagman, D. Parshall, M. B. Stone, A. T. Savici, Y. Zhao, H. A. Dabkowska, and B. D. Gaulin, Quasi-two-dimensional spin and phonon excitations in $La_{1.965}Ba_{0.035}CuO_4$, Phys. Rev. B **91**, 224404 (2015).

[44] M. Enoki, M. Fujita, T. Nishizaki, S. Iikubo, D. K. Singh, S. Chang, J. M. Tranquada, and K. Yamada, Spin-Stripe Density Varies Linearly with the Hole Content in Single-Layer $Bi_{2+x}Sr_{2-x}CuO_{6+y}$ Cuprate Superconductors, Phys. Rev. Lett. **110**, 017004 (2013).

[45] J. M. Tranquada, P. M. Gehring, G. Shirane, S. Shamoto, and M. Sato, Neutron-scattering study of the dynamical spin susceptibility in $YBa_2Cu_3O_{6.6}$, Phys. Rev. B **46**, 5561 (1992).

[46] D. Haug, V. Hinkov, Y. Sidis, P. Bourges, N. B. Christensen, A. Ivanov, T. Keller, C. T. Lin, and B. Keimer, Neutron scattering study of the magnetic phase diagram of underdoped $YBa_2Cu_3O_{6+x}$, New J. Phys. **12**, 105006 (2010).

[47] Pengcheng Dai, H. A. Mook, R. D. Hunt, and F. Doğan, Evolution of the resonance and incommensurate spin fluctuations in superconducting $YBa_2Cu_3O_{6+x}$, Phys. Rev. B **63**, 054525 (2001).

[48] S. Sugai, H. Suzuki, Y. Takayanagi, T. Hosokawa, and N. Hayamizu, Carrier-density-dependent momentum shift of the coherent peak and the LO phonon mode in p-type high-T_c superconductors, Phys. Rev. B **68**, 184504 (2003).

[49] M. Hücker, G. D. Gu, and J. M. Tranquada, Spin susceptibility of underdoped cuprate superconductors: Insights from a stripe-ordered crystal, Phys. Rev. B **78**, 214507 (2008).

[50] J. M. Tranquada, G. Shirane, B. Keimer, S. Shamoto, and M. Sato, Neutron scattering study of magnetic excitations in $YBa_2Cu_3O_{6+x}$, Phys. Rev. B **40**, 4503 (1989).

[51] R. R. P. Singh, Thermodynamic parameters of the T=0, spin-1/2 square-lattice Heisenberg antiferromagnet, Phys. Rev. B **39**, 9760 (1989).

[52] S. Shamoto, M. Sato, J. M. Tranquada, B. J. Sternlieb, and G. Shirane, Neutron-scattering study of antiferromagnetism in $YBa_2Cu_3O_{6.15}$, Phys. Rev. B **48**, 13817 (1993).

[53] S. Li, Z. Yamani, H. J. Kang, K. Segawa, Y. Ando, X. Yao, H. A. Mook, and P. Dai, Quantum spin excitations through the metal-to-insulator crossover in $YBa_2Cu_3O_{6+y}$, Phys. Rev. B **77**, 014523 (2008).

[54] O. J. Lipscombe, B. Vignolle, T. G. Perring, C. D. Frost, and S. M. Hayden, Emergence of Coherent Magnetic Excitations in the High Temperature Underdoped $La_{2-x}Sr_xCuO_4$ Superconductor at Low Temperatures, Phys. Rev. Lett. **102**, 167002 (2009).

[55] P. Bourges, H. F. Fong, L. P. Regnault, J. Bossy, C. Vettier, D. L. Milius, I. A. Aksay, and B. Keimer, High-energy spin excitations in **$YBa_2Cu_3O_{6.5}$**, Phys. Rev. B **56**, R11439 (1997).

[56] Pengcheng Dai, H. A. Mook, S. M. Hayden, G. Aeppli, T. G. Perring, R. D. Hunt, and F. Doğan, The magnetic excitation spectrum and thermodynamics of high-T_c superconductors, Science **284**, 1344 (1999).

[57] N. B. Christensen, D. F. McMorrow, H. M. Rønnow, B. Lake, S. M. Hayden, G. Aeppli, T. G. Perring, M. Mangkorntong, M. Nohara, and H. Tagaki, Dispersive Excitations in the High-Temperature Superconductor $La_{2-x}Sr_xCuO_4$, Phys. Rev. Lett. **93**, 147002 (2004).

[58] Guangyong Xu, G. D. Gu, M. Hucker, B. Fauque, T. G. Perring, L. P. Regnault, and J. M. Tranquada, Testing the itinerancy of spin dynamics in superconducting $Bi_2Sr_2CaCu_2O_{8+\delta}$, Nat. Phys. **5**, 642 (2009).

[59] C. Stock, W. J. L. Buyers, Z. Yamani, Z. Tun, R. J. Birgeneau, R. Liang, D. Bonn, and W. N. Hardy, Spin dynamics near the critical doping in weakly superconducting underdoped $YBa_2Cu_3O_{6.35}$ ($T_c = 18$ K), Phys. Rev. B **77**, 104513 (2008).

[60] N. S. Headings, S. M. Hayden, R. Coldea, and T. G. Perring, Anomalous High-Energy Spin Excitations in the High-T_c Superconductor-Parent Antiferromagnet La_2CuO_4, Phys. Rev. Lett. **105**, 247001 (2010).

[61] C. Stock, R. A. Cowley, W. J. L. Buyers, C. D. Frost, J. W. Taylor, D. Peets, R. Liang, D. Bonn, and W. N. Hardy, Effect of the pseudogap on suppressing high energy inelastic neutron scattering in superconducting $YBa_2Cu_3O_{6.5}$, Phys. Rev. B **82**, 174505 (2010).

[62] S. Hüfner, M. A. Hossain, A. Damascelli, and G. A. Sawatzky, Two gaps make a high-temperature superconductor? Rep. Prog. Phys. **71**, 062501 (2008).

[63] S. Pailhès, Y. Sidis, P. Bourges, V. Hinkov, A. Ivanov, C. Ulrich, L. P. Regnault, and B. Keimer, Resonant Magnetic Excitations

at High Energy in Superconducting $YBa_2Cu_3O_{6.85}$, Phys. Rev. Lett. **93**, 167001 (2004).

[64] L. Capogna, B. Fauque, Y. Sidis, C. Ulrich, P. Bourges, S. Pailhès, A. Ivanov, J. L. Tallon, B. Liang, C. T. Lin, A. I. Rykov, and B. Keimer, Odd and even magnetic resonant modes in highly overdoped $Bi_2Sr_2CaCu_2O_{8+\delta}$, Phys. Rev. B **75**, 060502(R) (2007).

[65] J. J. Wagman, J. P. Carlo, J. Gaudet, G. Van Gastel, D. L. Abernathy, M. B. Stone, G. E. Granroth, A. I. Kolesnikov, A. T. Savici, Y. J. Kim, H. Zhang, D. Ellis, Y. Zhao, L. Clark, A. B. Kallin, E. Mazurek, H. A. Dabkowska, and B. D. Gaulin, Neutron scattering studies of spin-phonon hybridization and superconducting spin gaps in the high-temperature superconductor $La_{2-x}(Sr, Ba)_xCuO_4$, Phys. Rev. B **93**, 094416 (2016).

[66] Hyungje Woo, A. T. Boothroyd, K. Nakajima, T. G. Perring, C. D. Frost, P. G. Freeman, D. Prabhakaran, K. Yamada, and J. M. Tranquada, Mapping spin-wave dispersions in stripe-ordered $La_{2-x}Sr_xNiO_4$ ($x = 0.275, 0.333$), Phys. Rev. B **72**, 064437 (2005).

[67] P. G. Freeman, A. T. Boothroyd, R. A. Ewings, M. Hücker, D. Prabhakaran, M. Enderle, and J. M. Tranquada, Temperature evolution of the magnetic excitations in charge ordered $La_{5/3}Sr_{1/3}NiO_4$, J. Phys: Condens. Matter **20**, 104229 (2008).

[68] M. Hücker, M. v. Zimmermann, G. D. Gu, Z. J. Xu, J. S. Wen, Guangyong Xu, H. J. Kang, A. Zheludev, and J. M. Tranquada, Stripe order in superconducting $La_{2-x}Ba_xCuO_4$ ($0.095 \leqslant x \leqslant 0.155$), Phys. Rev. B **83**, 104506 (2011).

[69] P. Bourges, Y. Sidis, H. F. Fong, L. P. Regnault, J. Bossy, A. Ivanov, and B. Keimer, The spin excitation spectrum in superconducting $YBa_2Cu_3O_{6.85}$, Science **288**, 1234 (2000).

[70] S. M. Hayden, H. A. Mook, Pengcheng Dai, T. G. Perring, and F. Doğan, The structure of the high-energy spin excitations in a high-transition-temperature superconductor, Nature (London) **429**, 531 (2004).

[71] S. D. Edkins, A. Kostin, K. Fujita, A. P. Mackenzie, H. Eisaki, S.-I. Uchida, S. Sachdev, M. J. Lawler, Eun-Ah Kim, J. C. Séamus Davis, and Mohammad H. Hamidian, Magnetic-field induced pair density wave state in the cuprate vortex halo, arXiv:1802.04673.

[72] E. Berg, E. Fradkin, S. A. Kivelson, and J. M. Tranquada, Striped superconductors: How spin, charge and superconducting orders intertwine in the cuprates, New J. Phys. **11**, 115004 (2009).

[73] D. R. Hamilton, G. D. Gu, E. Fradkin, and D. J. Van Harlingen, Signatures of pair-density wave order in phase-sensitive measurements of $La_{2-x}Ba_xCuO_4$-Nb Josephson junctions and SQUIDS, arXiv:1811.02048.

[74] E. Berg, E. Fradkin, and S. A. Kivelson, Charge-$4e$ superconductivity from pair-density-wave order in certain high-temperature superconductors, Nat. Phys. **5**, 830 (2009).

[75] Yangmu Li, J. Terzic, P. G. Baity, Dragana Popović, G. D. Gu, Qiang Li, A. M. Tsvelik, and J. M. Tranquada, Tuning from failed superconductor to failed insulator with magnetic field, arXiv:1810.10646.

[76] E. Fradkin, S. A. Kivelson, and J. M. Tranquada, Colloquium: Theory of intertwined orders in high temperature superconductors, Rev. Mod. Phys. **87**, 457 (2015).